Implementation of Self Contact in Path Generating Compliant Mechanisms

Prabhat Kumar, Anupam Saxena and Roger A. Sauer

Abstract Path generating compliant mechanisms with self contact are synthesized using continuum discretization and negative circular masks. Hexagonal cells are employed to represent the design space and negative circular masks are used to remove material beneath them. Each mask is defined by three parameters which constitute the design vector, which is mutated using the Hill-climber search. Hexagonal cells circumvent various geometrical singularities related to single point connections however, many "V" notches get retained on the boundary edges. Self contact is permitted between various subregions of the continuum. To achieve convergence in contact analysis, it is essential to have smooth boundary surfaces for which a smoothing technique is employed. Consequently, many hexagonal cells get modified to six-noded generic polygons. Non-linear finite elements analysis is implemented with Mean Value Coordinates based shape functions. Self contact is modeled between two deformable bodies in association with augmented Lagrange multiplier method. To minimize the error in shape, size and orientation between the actual and specified paths, a Fourier Shape Descriptors based objective is employed. An example of path generating compliant mechanism which experiences self contact is presented and its performance is compared with a commercial software.

Keywords Complaint mechanisms · Self contact · Mean value coordinates · Boundary smoothing · Fourier shape descriptors

P. Kumar (✉) · A. Saxena
Indian Institute of Technology Kanpur, Kanpur, India
e-mail: kprabhat@iitk.ac.in

A. Saxena
e-mail: anupams@iitk.ac.in

R.A. Sauer
RWTH Aachen University, Aachen, Germany
e-mail: sauer@aices.rwth-aachen.de

1 Compliant Mechanisms

Compliant mechanisms (CMs) execute the desired work by deriving the mobility from the deflection of their deformable members. Such deflections may be large or small depending upon their applications. CMs assure various advantages e.g., ease in assembly and manufacturing, less wear and frictional losses, more precision and no backlash. Consequently, use of such mechanisms is increasing in the different engineering domains e.g., micro-electro-mechanical systems, aerospace, automotive, bio-medical devices and various other fields.

To synthesize compliant mechanisms, two well established approaches e.g., topology optimization (Bendsøe and Kikuchi 1988; Sigmund 1997) and Pseudo Rigid Body Models (Howell 2001) exist. Topology optimization entails systematic determination of the material layout via extremising a certain objective with/without some constraints. Methods that employed quadrilateral cells to discretize the design domain suffer from many geometrical singularities (Saxena 2011) mostly related to the point connection between two neighboring elements. Hexagonal cells have natural edge connectivity between two neighboring cells (Saxena 2011). To perform finite element analysis, each hexagonal cell is either divided into six triangular elements (Langelaar 2007), or two quadrilateral shapes (Saxena and Saxena 2007), or modeled as a single element (Saxena 2011).

For path generating CMs, to minimize the discrepancies in the specified and actual paths, objective based on least-square is used (Saxena and Ananthasuresh 2001). Least-square objective does not provide local control for discrepancies in shape, size and orientation of paths. Fourier shape descriptors (FSDs) based objective is employed by Ullah and Kota (1997) to compare individual discrepancies in the shape, size and orientation of paths.

Non smooth paths can be generated either using partial compliant (Rai et al. 2007) or contact-aided compliant mechanisms (Mankame and Ananthasuresh 2004). Prespecified contact surfaces were used in association with FSDs objective (Mankame and Ananthasuresh 2004). Pseudo hinges/sliding pairs (Kumar et al. 2016) get introduced at mating surfaces and consequently configurations (Midha et al. 1994) of CMs change. Reddy et al. (2012) used curve beams to discretize the design space and determined contact locations systematically rather than pre-specifying them to synthesize non-smooth path generating contact-aided compliant mechanism. Kumar et al. (2016) presented continuum discretization based approach to synthesize C^0 path generating contact-aided compliant mechanisms with mutual contact.

2 Motivation

Constituting members of CMs while undergoing large deformation may experience self contact, which is implemented herein. Hexagonal cells are used to represent the design space and negative circular masks are placed suitably over it to remove material within cells beneath the overlaying masks to impart the optimum material layout.

Contents of the paper are organized as follows: Sect. 3 briefs the continuum discretization and topology optimization with negative circular masks. Boundary smoothing and finite element formulation are discussed in Sect. 4. Section 5 outlines contact modeling and analysis. An example on path generating contact-aided compliant mechanism is presented in Sect. 6 followed by the concluding remarks in Sect. 7.

3 Continuum Discretization and Negative Circular Masks

A tessellation of hexagonal cells (Ω_H) represent the design domain and negative circular masks (Ω_M) are employed to assign the material state $\rho(\Omega_H)$ to each cell. Each mask is modeled with three parameters (x_i, y_i, r_i) which constitute the design vector, where r_i is the radius of the ith mask and (x_i, y_i) are the coordinates of its center. If N masks are employed, the design vector contains $3N$ parameters. $\rho_k(\Omega_H) = 0$ implies cell is void, while $\rho_k(\Omega_H) = 1$ represents solid cell. A compliant continuum therefore comprises of all unexposed cells. The boundary of such continua contains many V-notches which pose difficulty in manufacturing, generate stress-concentration regions, and importantly, pose difficulty in convergence of contact analysis (Kumar and Saxena 2015). Mathematically, the material states of any cell can be described as

$$\rho(\Omega_H) = \begin{cases} 0, & \text{if } \Omega_H^c \subset \text{ any } \Omega_M(d_{ik} - r_i \leq 0) \\ 1, & \text{if } \Omega_H^c \not\subset \text{ any } \Omega_M(d_{ik} - r_i > 0) \end{cases} \tag{1}$$

where Ω_H^c represents the centroid of Ω_H, and d_{ik} is the distance between the centers of Ω_M and Ω_H^c (Fig. 1).
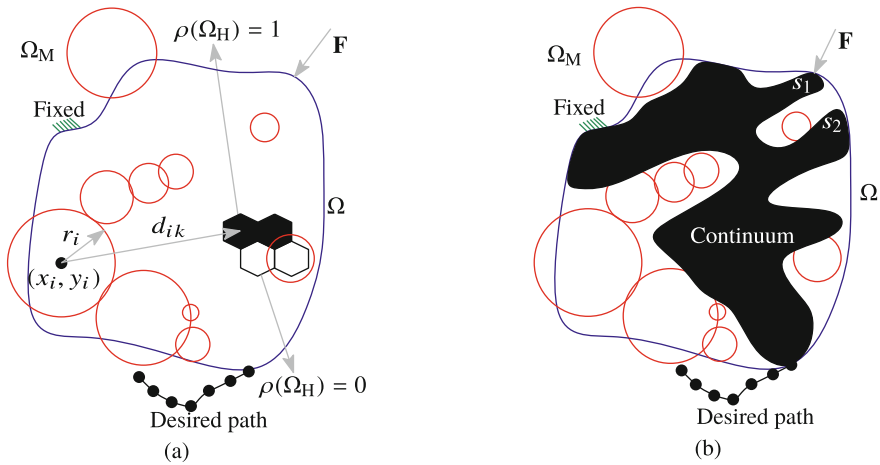
Fig. 1 Hexagonal cells Ω_H are used to discretize the design space Ω (*blue curve*) and negative masks Ω_M (*red circles*) are placed over them. Unexposed cells comprise the continuum (*black solid* in (**b**)). Input force (**F**), desired output path (*black curve* with *dots*) and fixed boundaries are shown. Surfaces s_1 and s_2 (shown in (**b**)), and many such surface pairs, may come in contact

4 Boundary Smoothing and Finite Element Formulation

The obtained final compliant continua by the use of hexagonal cells and negative circular masks contain serrated bounding surfaces (Kumar and Saxena 2015). However, to facilitate contact analysis, it is desirable to have smooth bounding surfaces (Corbett and Sauer 2014). Thus, boundary smoothing scheme is implemented herein to smoothen the bounding surfaces. In this section, we briefly present boundary smoothing scheme and finite element formulation.

4.1 Boundary Smoothing

Boundary smoothing (Kumar and Saxena 2015) is employed to alleviate V notches at the continuum boundary(ies) resulting due to hexagonal cells. Bounding edges of the continuum and boundary nodes are noted. Mid-points of these edges are joined via straight lines. Boundary nodes are projected to these lines along their shortest perpendiculars (Fig. 2a). Positions of boundary nodes are updated and used for finite element analysis. The connectivity matrix remain unchanged. The smoothing process can be implemented multiple times (Fig. 2b). The process may alter some of hexagonal cells into six-noded generic concave polygons (as shown in Fig. 2b). The continuum volume can be reduced further by removing regular cells, i.e., those do not get affected by boundary smoothing. This is equivalent to introducing more
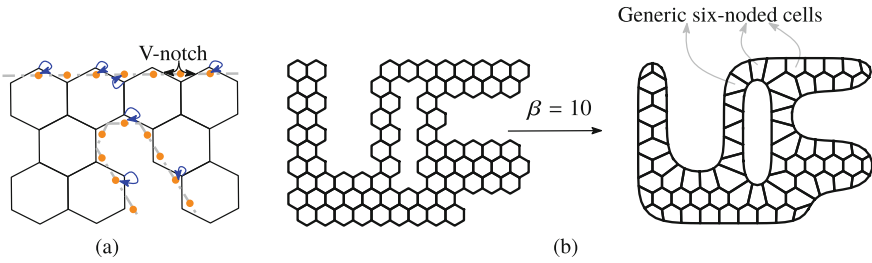
Fig. 2 Boundary smoothing **a** boundary nodes are projected along their shortest perpendiculars on *straight lines* joining mid-points of boundary edges **b** *left* with $\beta = 0$ and *right* with $\beta = 10$. β : number of boundary smoothing steps

negative masks, one for each regular cell, such that the centers of that respective cell and the mask coincide. Smoothing is performed again to eliminate the remnant notches.

4.2 Finite Element Formulation

The boundary smoothing process (Kumar and Saxena 2015) results in altering some regular hexagonal cells into six-noded generic polygonal cells. These cells are modeled with Mean Value Coordinates based shape functions (Floater 2003; Sukumar and Tabarraei 2004). Elemental stiffness matrix $\mathbf{K}_e$ is evaluated as follows: (i) Each cell is divided into six triangular regions with respect to the centroid of that cell. (ii) Integration over each triangle is performed with 25 Gauss-points[1] (Kumar and Saxena 2015). (iii) Summation of such six integrations is done and $\mathbf{K}_e$ is obtained. The global stiffness matrix $\mathbf{K}^{glob}$ is evaluated by assembling $\mathbf{K}_e$. Likewise the internal force vector $\mathbf{r}_e$ and global internal force vector $\mathbf{R}$ are obtained. When self contact arises the elemental contact force $\mathbf{f}_c^e$ and corresponding stiffness $\mathbf{K}_c^e$ are evaluated, as below, and placed at their global degree of freedom inside $\mathbf{R}$ and $\mathbf{K}^{glob}$.

5 Contact Modeling and Analysis

Self contact is modeled as quasi-static contact between two deformable bodies in association with augmented Lagrange multiplier method.

---

[1]for accuracy.

Consider two deformable bodies $\mathcal{B}_{01}$ and $\mathcal{B}_{02}$, in their undeformed configurations, to come in contact in their current (deformed) configurations[2]. The weak form (Sauer and De Lorenzis 2013) can be written as

$$\delta\Pi(\boldsymbol{\phi}, \delta\boldsymbol{\phi}) = \delta\Pi_{\text{int}} + \delta\Pi_{\text{c}} - \delta\Pi_{\text{ext}} = 0 \quad \forall \delta\boldsymbol{\phi} \subset \gamma \tag{2}$$

where $\boldsymbol{\phi} = (\boldsymbol{\phi_1}, \boldsymbol{\phi_2})$ is the deformation field for $\mathcal{B}_1$ and $\mathcal{B}_2$ respectively and the virtual displacement field $\delta\boldsymbol{\phi}(\delta\boldsymbol{\phi_1}, \delta\boldsymbol{\phi_2})$ is defined in the space γ of all kinematically permissible deformations. $\delta\Pi_{\text{int}}$, $\delta\Pi_{\text{c}}$ and $\delta\Pi_{\text{ext}}$ are internal, contact and external virtual works respectively. The virtual contact work $\{\delta\Pi_c = \delta\Pi_{c1} + \delta\Pi_{c2}\}$ (Sauer and De Lorenzis 2013) is defined as

$$\delta\Pi_{ck} = - \int\limits_{\delta_c \mathcal{B}_k} \mathbf{t}_k . \delta\boldsymbol{\phi}_k da_k, \tag{3}$$

where $\delta_c\mathcal{B}_k$ is the contact surface, $\mathbf{t}_k$ is the contact traction and a_k is the contact surface area. Further, indices c and k are used to represent contact and two deformable bodies respectively.

5.1 Normal Contact

Consider two points $P_1(\mathbf{x}_1)$ and $P_2(\mathbf{x}_2)$ on bodies $\mathcal{B}_1$ and $\mathcal{B}_2$ respectively[3] (Fig. 3b). The gap between them is defined as

$$\mathbf{g} = \mathbf{x}_2 - \mathbf{x}_1. \tag{4}$$

If $\mathbf{g}.\mathbf{n}_1 \geq 0$, bodies do not penetrate each other. Here $\mathbf{n}_1$ is the normal vector at $P_1(\mathbf{x}_1)$. The distance d between points is $||\mathbf{x}_2 - \mathbf{x}_1||$. For a given $\mathbf{x}_2 \subset \partial\mathcal{B}_2$, we search for a point $\mathbf{x}_1 \subset \partial\mathcal{B}_1$ such that d becomes *minimum*. That is, we solve for

$$d_{min} = \min_{\mathbf{x}_1 \subset \mathcal{B}_1} (d) \tag{5}$$

We assume that the boundary surfaces are convex locally. Each material point on $\mathcal{B}_1$ is defined using a convective co-ordinates system $\boldsymbol{\xi} = (\xi^1, \xi^2)$, with $\frac{\partial\mathbf{x}_1}{\partial\xi^\alpha} = \mathbf{a}_\alpha^1; \alpha = 1, 2$. Here $\mathbf{a}_\alpha^1$ is the tangent vector. The solution of Eq. (5) is obtained by imposing $\frac{\partial d}{\partial\xi^\alpha} = 0$. Since $\frac{\partial d}{\partial\xi^\alpha} = \left\{\frac{\partial d}{\partial\mathbf{x}_1} . \frac{\partial\mathbf{x}_1}{\partial\xi^\alpha}\right\}$, the following two conditions are obtained

---

[2]bodies are denoted as $\mathcal{B}_1$ and $\mathcal{B}_2$.

[3]$P_1(\mathbf{X}_1)$ and $P_2(\mathbf{X}_2)$ are the corresponding points in the undeformed configurations respectively.
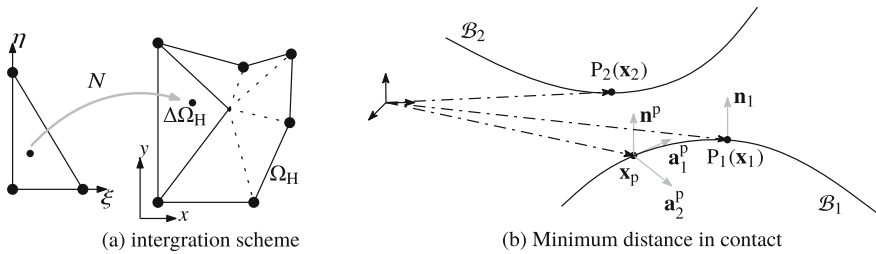
(a) intergration scheme   (b) Minimum distance in contact

Fig. 3 **a** Each cell is divided into six Δ regions and integration is performed. **b** Points of surfaces coming in contact are determined by finding the minimum distance between them

$$\frac{\partial d}{\partial \xi^{\alpha}} = -\{\mathbf{x}_2 - \mathbf{x}_1(\boldsymbol{\xi})\}.\mathbf{a}_{\alpha}^1 = 0 \tag{6}$$

Let Eq. (6) holds true for $\mathbf{x}_1(\boldsymbol{\xi})|_{\boldsymbol{\xi}=\boldsymbol{\xi}_p} = \mathbf{x}_p(\boldsymbol{\xi}_p)$, where at $\mathbf{x}_p$, $\mathbf{a}_{\alpha}^p$ and $\mathbf{n}^p$ are the tangent and normal vectors respectively. The normal gap is evaluated as

$$g_n = (\mathbf{x}_2 - \mathbf{x}_p(\boldsymbol{\xi}_p)).\mathbf{n}^p. \tag{7}$$

For discrete surfaces (C^0 continuous), surface normals vary at each nodal position. Therefore, for such surfaces, normal is equivalent to

$$\mathbf{n}^p = (\mathbf{x}_2 - \mathbf{x}_p(\boldsymbol{\xi}_p))/g_n \tag{8}$$

where normal gap $g_n = \pm\sqrt{(\mathbf{x}_2 - \mathbf{x}_p).(\mathbf{x}_2 - \mathbf{x}_p)}$. In classical penalty method (Sauer and De Lorenzis 2013), traction $\mathbf{t}_{ck}$ is defined as

$$\mathbf{t}_{ck} = \begin{cases} -\varepsilon_n g_n \mathbf{n}^p & \text{for } g_n < 0 \\ \mathbf{0} & \text{for } g_n \geq 0 \end{cases} \tag{9}$$

where ϵ_n is a chosen penalty parameter.

5.2 Contact Discretization

We employ, the following 2D linear Lagrangian basis functions to represent contact segments.

$$N_{pk}^1 = \frac{1}{2}(1 - \xi_P^k), \quad N_{pk}^2 = \frac{1}{2}(1 + \xi_P^k) \tag{10}$$

where $\xi_p^k|\,(k=1,2)$ is obtained by solving Eq. (6). The contact virtual work in the discretized system is defined as

$$\delta\Pi_{ck} \cong \delta\Pi_{ck}^h = \sum_{e=1}^{n_{sel}} \delta\Pi_{ck}^e \tag{11}$$

where n_{sel} is the number of surface elements Γ^e in the discretized contact segment $\partial_c\mathcal{B}_k^h$. We rewrite Eq. (3) in the discretized segments $\partial_c\mathcal{B}_k^h$ correspond to $\delta_c\mathcal{B}_k$ as

$$\delta\Pi_{ck}^e = -\int_{\Gamma^e} \delta\boldsymbol{\phi}_{ck}^e \cdot \mathbf{t}_{ck} da_k; \quad k=1,2 \tag{12}$$

where $\delta\boldsymbol{\phi}_{ck}^e = \mathbf{N}_{ck}v_{ck}^e$ and $\mathbf{N}_{ck}$ equals $[N_{pk}^1\mathbf{I}_2, N_{pk}^2\mathbf{I}_2]$ with $\mathbf{I}_2$ is 2×2 unit matrix and v_{ck}^e is the virtual displacement vector. Therefore, Eq. (12) is equivalent to

$$\delta\Pi_{ck}^e = -v_{ck}^e \int_{\Gamma^e} \mathbf{N}_{ck}^T \mathbf{t}_{ck} da_k; \quad k=1,2 \tag{13}$$

From Eq. (13) the elemental contact force vector is evaluated as

$$\mathbf{f}_{ck}^c = -\int_{\Gamma^e} \mathbf{N}_{ck}^T \mathbf{t}_{ck} da_k; \quad k=1,2 \tag{14}$$

and thus, elemental contact stiffness matrix is calculated as

$$\mathbf{K}_{ck}^e = \frac{\partial \mathbf{f}_{ck}^e}{\partial \mathbf{u}_k^e} = -\int_{\Gamma^e} \mathbf{N}_{ck}^T \frac{\partial \mathbf{t}_{ck}}{\partial \mathbf{u}_k^e} da_k = -\int_{\Gamma^e} \mathbf{N}_{ck}^T \frac{\partial \mathbf{t}_{ck}}{\partial \mathbf{x}_k^e} \mathbf{N}_{ck} da_k, \tag{15}$$

where elemental displacement vector $\mathbf{u}_k^e = \mathbf{x}_k^e - \mathbf{X}_k^e$. Detailed expressions for contact force vector and elemental contact stiffness are mentioned in (Sauer and De Lorenzis, 2013). We have considered frictionless contact in our implementation.

6 Synthesis Example

We present an example where the compliant mechanism experiences self contact (Fig. 4b) while tracing the specified path. To attain this CM, the objective (Kumar et al. 2016) based on Fourier Shape Descriptors with the given volume constraint is minimized using the Random Mutation Hill Climber method (Kumar et al. 2016). Table 1 depicts the value of different parameters used in the optimization process. Figure 4a describes the design specifications for the compliant continuum. The CM
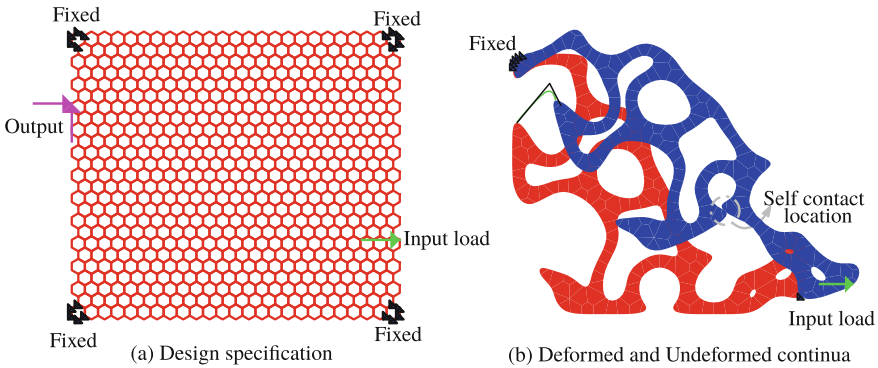
Fig. 4 **a** Design Specifications are shown. **b** The undeformed (*red in color*) and deformed (*blue in color*) configurations are shown. *Dotted-circle* is the zone of self contact. The specified path (*black*) and the actual path (*green*) is also shown

Table 1 Parameters used in the synthesis. *HCH* and *HCV* represent the number of hexagonal cells in the horizontal directions and in the vertical direction respectively

Parameter's name	Value	Parameter's name	Value
Design domain ($HCH \times HCV$)	25 × 25	Number of Ω_M in x-direction (N_x)	7
Number of Ω_M in y-direction (N_y)	7	Maximum radius of Ω_M	6.0 mm
Minimum radius of Ω_M	0.1 mm	Maximum number of iterations	40,000
Young's modulus	2100 MPa	Poisson's ratio	0.30
Permitted volume fraction ($\frac{V*}{V}$)	0.30	Mutation probability	0.08
Contact surface radii factor	0.50	Maximum mutation size (m_{max})	6
Upper limit for input load	500 N	Lower limit for input load	−500 N
Weight for A_{err} (w_a)	50	Weight for B_{err} (w_b)	50
Weight for path length error (w_L)	1	Weight for path orientation error (w_q)	5
Boundary smoothing steps (β)	10	Penalty parameter (ε_n)	100

is also analyzed in Abaqus with neo-Hookean material and four-noded plain-strain elements (CPE4I) using the obtained optimal force, boundary conditions, and active self contact locations. The actual path traced by the CM using presented method closely follows the path obtained via Abaqus analysis (Fig. 5c).

Figure 4b depicts the deformed (in blue) and undeformed (in red) configurations of the final optimized compliant continuum. Two intermediate configurations of the CMs, one before contact and one after, are shown in 5a and 5b while tracing the path (green in color). Figure 5c compares the specified, actual and that obtained using Abaqus. The final compliant mechanism is obtained after 5741 search iterations with 104.61 N input force.
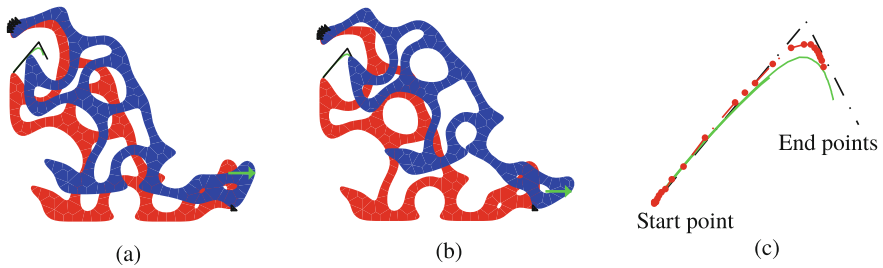
Fig. 5 Intermediate deformed configurations of CMs are shown in **a**, and **b**. **c** Compares the specified path (*black in color*) and the actual path (*green in color*) and that using Abaqus (*red dash-dotted*)

7 Conclusion

We present a continuum discretization based method to design the optimal topology of a compliant mechanism undergoing self contact. Hexagonal cells are employed for domain representation and negative masks are used for material assignment. Boundary smoothing is used to facilitate contact analysis. Mean Value Coordinates based shape functions are employed for Finite Element Analysis. Hill climber search process is used to optimize the Fourier Shape Descriptors objective to achieve the specified path. Contact-aided compliant mechanisms may find use in special purpose applications, say static balancing, negative stiffness etc. One can also implement both self contact and mutual (two different bodies) contact, a goal, planned for future work.

References

Bendsøe MP, Kikuchi N (1988) Generating optimal topologies in structural design using a homogenization method. Comput Methods Appl Mech Eng 71(2):197–224

Corbett CJ, Sauer RA (2014) Nurbs-enriched contact finite elements. Comput Methods Appl Mech Eng 275:55–75

Floater MS (2003) Mean value coordinates. Comput Aided Geom Des 20(1):19–27

Howell LL (2001) Compliant mechanisms. Wiley, New York

Kumar P, Saxena A (2015) On topology optimization with embedded boundary resolution and smoothing. Struct Multi Optim 52(6):1135–1159

Kumar P, Sauer RA, Saxena A (2016) Synthesis of c0 path-generating contact-aided compliant mechanisms using the material mask overlay method. J Mech Des 138(6):062301

Langelaar M (2007) The use of convex uniform honeycomb tessellations in structural topology optimization. In: 7th world congress on structural and multidisciplinary optimization, Seoul, South Korea, pp 21–25

Mankame ND, Ananthasuresh G (2004) Topology optimization for synthesis of contact-aided compliant mechanisms using regularized contact modeling. Comput Struct 82(15):1267–1290

Midha A, Norton TW, Howell LL (1994) On the nomenclature, classification, and abstractions of compliant mechanisms. J Mech Des 116(1):270–279

Rai AK, Saxena A, Mankame ND (2007) Synthesis of path generating compliant mechanisms using initially curved frame elements. J Mech Des 129(10):1056–1063

Reddy BN, Naik SV, Saxena A (2012) Systematic synthesis of large displacement contact-aided monolithic compliant mechanisms. J Mech Des 134(1):011007

Sauer RA, De Lorenzis L (2013) A computational contact formulation based on surface potentials. Comput Methods Appl Mech Eng 253:369–395

Saxena A (2011) Topology design with negative masks using gradient search. Struct Multi Optim 44(5):629–649

Saxena A, Ananthasuresh G (2001) Topology synthesis of compliant mechanisms for nonlinear force-deflection and curved path specifications. J Mech Des 123(1):33–42

Saxena R, Saxena A (2007) On honeycomb representation and sigmoid material assignment in optimal topology synthesis of compliant mechanisms. Finite Elem Anal Des 43(14):1082–1098

Sigmund O (1997) On the design of compliant mechanisms using topology optimization*. J Struct Mech 25(4):493–524

Sukumar N, Tabarraei A (2004) Conforming polygonal finite elements. Int J Numer Meth Eng 61 (12):2045–2066

Ullah I, Kota S (1997) Optimal synthesis of mechanisms for path generation using fourier descriptors and global search methods. J Mech Des 119(4):504–510